PROCEEDINGS OF SPIE

SPIEDigitalLibrary.org/conference-proceedings-of-spie

Exploring the potential of cycloidal computed tomography for advancing intraoperative specimen imaging

Roche i Morgo, Oriol, Massimi, Lorenzo, Suaris, Tamara, Endrizzi, Marco, Munro, Peter R., et al.

Oriol Roche i Morgo, Lorenzo Massimi, Tamara Suaris, Marco Endrizzi, Peter R. T. Munro, Savvas Savvidis, Glafkos Havariyoun, P. M. Sam Hawker, Alberto Astolfo, Oliver J. Larkin, Rachel L. Nelan, J. Louise Jones, Daniël M. Pelt, David Bate, Alessandro Olivo, Charlotte K. Hagen, "Exploring the potential of cycloidal computed tomography for advancing intraoperative specimen imaging," Proc. SPIE 11840, Developments in X-Ray Tomography XIII, 118400R (9 September 2021); doi: 10.1117/12.2594547

SPIE.

Event: SPIE Optical Engineering + Applications, 2021, San Diego, California, United States

Exploring the potential of cycloidal computed tomography for advancing intraoperative specimen imaging

Oriol Roche i Morgó,*[a] Lorenzo Massimi,[a] Tamara Suaris,[b] Marco Endrizzi,[a] Peter R. T. Munro,[a] Savvas Savvidis,[a] Glafkos Havariyoun,[a] P. M. Sam Hawker,[c] Alberto Astolfo,[a,c] Oliver J. Larkin,[c] Rachel L. Nelan,[d] J. Louise Jones,[b,d] Daniël M. Pelt,[e] David Bate,[a,c] Alessandro Olivo,[a] Charlotte K. Hagen[a]

[a]Dept. of Medical Physics and Biomedical Engineering, University College London, Gower St, London WC1E 6BT, UK; [b]St Bartholomew's Hospital, Barts Health NHS Trust, West Smithfields, London EC1A 7BE, UK; [c]Nikon X-Tek Systems, Tring Business Centre, Icknield Way, Tring, Hertfordshire, HP23 4JX, UK; [d]Barts and the London School of Medicine and Dentistry, Queen Mary University of London, Newark St, London E1 2AT, UK; [e]Leiden Institute of Advanced Computer Science, Leiden University, Niels Bohrweg 1, 2333 CA, Leiden, The Netherlands

ABSTRACT

A preliminary investigation into the use of cycloidal computed tomography for intraoperative specimen imaging is presented. Intraoperative imaging is applied in time-sensitive clinical settings, where obtaining a high-resolution, high-quality image within minutes is paramount in evaluating the success of operations and/or the need for additional surgery. As a flexible imaging method that is compatible with x-ray phase contrast imaging, cycloidal computed tomography can provide both high spatial resolution and high image contrast, whilst keeping scan times short thanks to an effective under-sampling approach. To gather early evidence, the method was tested on resected breast and oesophageal tissue. The results, although preliminary, indicate that cycloidal imaging may indeed be beneficial for intraoperative specimen imaging, although further studies are required to confirm this potential.

Keywords: cycloidal computed tomography, micro computed tomography, spatial resolution, x-ray imaging, intraoperative specimen imaging, spatial resolution, structured illumination, phase contrast, edge illumination

1. INTRODUCTION

Tumour-bearing tissue is routinely imaged in-theatre to establish whether a lesion was completely removed leaving an unaffected tissue margin[1]. Planar radiography is used, but contrast is low due to small differences in the x-ray attenuation of diseased and healthy tissue, which, together with the 2D nature of the images, results in relatively poor performance[2].

Our group has developed dedicated x-ray phase contrast micro-computed tomography (CT) scanners for the intraoperative margin assessment of resected tumours[3-5]. These implement "edge-illumination" (EI), utilising masks to generate separated x-ray beamlets and analyse their refraction. While initial results are promising, the resolution of these scanners has so far been constrained by the need to meet clinically workable scan times (minutes).

We have developed a new acquisition method ("cycloidal CT") by which our scanners' resolution could potentially be increased without extending scan time[6]. In this method, the sample is translated in the lateral plane as it rotates, which alleviates the under-sampling imposed by the beamlets. Cycloidal sampling, which derives its name from the trajectory followed by any point in the sample during this "roto-translation" motion, does not involve the acquisition of more data, but leads to a more even sampling of the sinogram. "Gaps" in the latter can be completed via, e.g., interpolation or machine learning.

*oriol.roche.15@ucl.ac.uk

Developments in X-Ray Tomography XIII, edited by Bert Müller
Ge Wang, Proc. of SPIE Vol. 11840, 118400R · © 2021 SPIE
CCC code: 0277-786X/21/$21 · doi: 10.1117/12.2594547

Here, we report first results of applying the principles of cycloidal CT to two types of biological tissue with relevance to intraoperative specimen imaging, breast and oesophagus. Breast conserving surgery is one of the primary treatment options for breast cancer[7,8]. Oesophagectomies are performed to remove oesophageal cancer that has not spread beyond the local area[9,10].

The images presented here were obtained with our breadboard setup in the UCL labs, rather than with the dedicated intraoperative scanners referred to above. However, we believe that our results will be instrumental to guiding a possible future implementation of the cycloidal method in those scanners.

2. METHODS

2.1 Edge-illumination x-ray phase contrast imaging

X-ray phase contrast imaging differs from conventional, attenuation-based x-ray imaging in that phase shifts and/or refraction contribute to the image formation[11,12]. Experimental studies have demonstrated the ability of x-ray phase contrast imaging to yield a higher contrast-to-noise ratio (CNR) than conventional attenuation-based x-ray imaging. In particular, this applies to samples with weak intrinsic x-ray attenuation such as soft biological tissue[13-16], a category that includes surgically excised human tissue, which explains why the technology is receiving attention in the context of intraoperative specimen imaging[3-5,17].

While x-ray phase contrast imaging has traditionally relied on coherent synchrotron radiation, the "edge-illumination" (EI) x-ray phase contrast technique is one of few methods with relaxed coherent requirements[18-21]. Consequently, it can be implemented with lab-based x-ray tubes, making it suitable for in-theatre use. In brief, EI is based on using a mask ("sample mask") with periodically spaced slit-shaped apertures to structure the x-ray beam into an array of narrow beamlets. A second mask ("detector mask"), placed immediately before the detector, creates insensitive areas in between pixels (see Fig. 1a)[18,22]. By offsetting the two masks in such a way that only part of each beamlet reaches an active pixel area, sensitivity to small directional changes of the beamlets is created, as these translate into a higher or lower detected intensity. In other words, the detector mask acts as an analyser for x-ray refraction. The mask offset is typically chosen such that it coincides with one of the slopes of the illumination curve[23,24] (see Fig. 1b). The illumination curve is obtained in the absence of the sample by translating the sample mask, in subpixel increments, by a full mask period and measuring the intensity.

While, as mentioned, x-ray phase contrast imaging can provide a high CNR, this is not the only metric to consider when evaluating image quality. Spatial resolution is equally important, especially when the imaging task is to visualise tumour margins in surgically excised tissue. In EI, spatial resolution is, to first approximation, determined by the width of the sample mask apertures; however, this can only translate into an equally high resolution in the images if signals are adequately sampled[25,26]. The use of narrow beamlets, separated by distances of typically 3-10 times their width, implies that signals are sampled substantially below the Nyquist rate, unless a process called "dithering" is applied. In dithering, the sampling rate is increased by taking multiple exposures, each with the sample in a different subpixel position. This is time-consuming, especially when performing CT scans given that dithering must be applied at each rotational position of the sample. Consequently, dithering may not be an option in intraoperative specimen imaging where scan times need to be kept at a minimum.

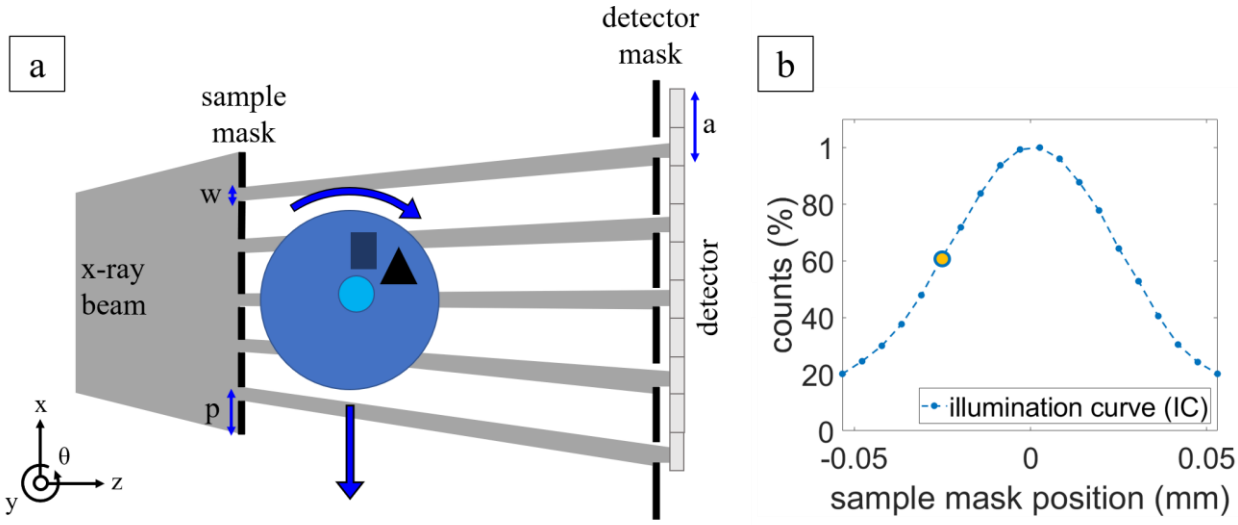

Figure 1. Panel (a) shows a schematic of an EI x-ray imaging setup. The sample mask period *p* and aperture *w* match the period and aperture of the detector mask, adjusted for magnification. This is a "line skipping" setup, where the period of the detector mask matches the length of 2 pixels so that every other pixel column is covered. These masks are employed to effectively reduce crosstalk in the detector. Panel (b) shows an example of an illumination curve, obtained by scanning the sample masks by one period in several subpixel steps and recording the changes in intensity at the detector. The yellow dot shows the point of maximum slope, which is commonly selected for imaging.

2.2 Cycloidal computed tomography

Cycloidal computed tomography[6,27] refers to an imaging concept by which the abovementioned under-sampling problem is alleviated in a different manner. Rather than step-scanning the sample for each rotational position, as is done in dithering, the sample is translated *as it rotates*. This means that at each rotational position the sample is also in a different lateral (subpixel) position, hence different parts of the sample are captured in each projection.

Although the cycloidal sampling trajectory does not *solve* the under-sampling problem, as no additional data points are acquired, the scheme leads to a "spreading out" of the sampled data across the sinogram domain. This is illustrated in Fig. 2; panel (a) shows how the sinogram is sampled through dithering (i.e. a complete dataset is acquired), panel (b) shows the sinogram sampling obtained by only rotating the sample without applying dithering ("rotation-only"), and panel (c) shows the grid resulting from cycloidal sampling. Previous work has shown that an even coverage of the sinogram, as can be seen in panel (c), provides a favourable configuration for recovering the missing data using mathematical methods[6]. Simulations and experimental results suggest that cycloidal CT can yield a resolution comparable to dithering without having to apply time-consuming step-scanning of the sample at each rotational position[27].

Cycloidal CT can be implemented in any scanner in which the x-ray beam is split into narrow beamlets, so long as the beamlets are sufficiently spatially separated. While this demands that a mask or similar beam-shaping structure is placed upstream of the sample, the usage of a detector mask is not necessarily required. In fact, the detector mask can be considered as a means for flexibly swapping between contrast modes; without it, the recorded signals are almost entirely generated by x-ray attenuation, whereas, with the detector mask in place, additional and complementary sensitivity to refraction is achieved.

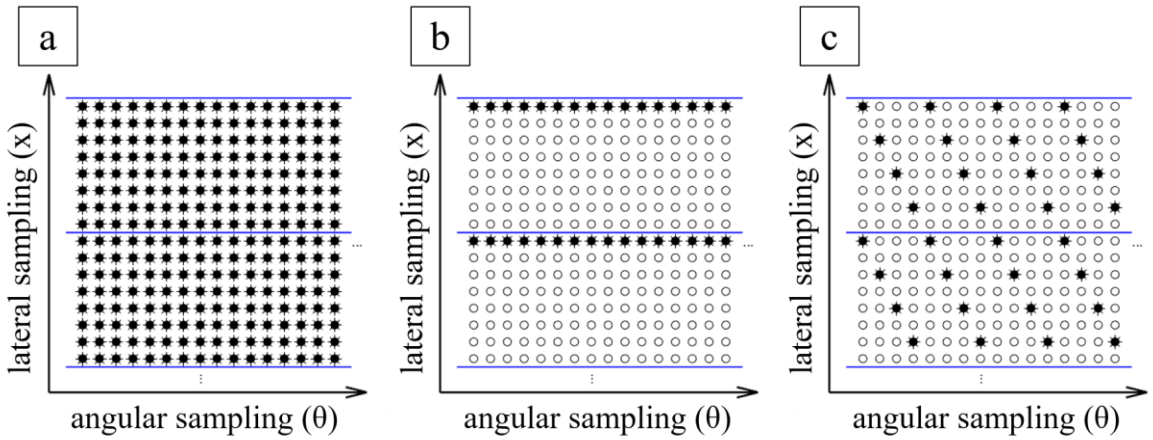

Figure 2. Schematics illustrating the sampling of the sinogram space for different acquisition strategies (shown for two mask periods and a subset of rotation angles). The blue lines represent the boundaries of the sample mask periods, or the pixel size (de-magnified). The black, full circles represent the acquired data points. Panel (a) represents a dithered case, where frames are acquired at several subpixel positions (generally, enough to abide by the Nyquist frequency, although this can change depending on the resolution needs of the scan). Panel (b) represents the rotation-only case, where the sample simply rotates with no lateral translation. Panel (c) presents the cycloidally sampled case, with the data spread out across the sinogram. Panels (b) and (c) have the same amount of data, but the distribution in the cycloidal case provides a more favourable basis for high resolution reconstructions.

2.3 Image reconstruction in cycloidal computed tomography

Since cycloidal signals are under-sampled, a data recovery step is needed before tomographic images can be reconstructed. This is to "fill in" the missing data points in the sinogram (i.e. the "empty" circles in Fig. 2c). Data recovery can be performed with a variety of methods. Initially we used bicubic splines to interpolate under-sampled cycloidal sinograms, due to their availability as in-built functions in standard image processing software[6,27]. More recently, we have integrated a convolutional neural network (CNN) layer into the processing, which utilises learned relationships between interpolated and dithered data to improve image quality[28].

If cycloidal data are acquired in phase contrast mode (i.e. with the detector mask in place), phase retrieval must be applied following the recovery of the sinogram in order to "isolate" the phase function, which has a known line integral relationship with the decrement of unity from the real part of the complex refractive index n, defined as:

$$n(\mathrm{E}) = 1 - \delta(\mathrm{E}) + \mathrm{i}\beta(\mathrm{E})$$

where δ is linked to phase effects, β is linked to attenuation, and E is the photon energy. Traditionally in EI, phase retrieval has relied on the acquisition of two or more projections at different illumination curve positions for each rotational position of the sample[29]. More recently, we developed a "single-shot" approach where only one projection is required[30,31]. This method is derived from two assumptions; (1) refraction angles must be small, and (2) the sample must be quasi-homogeneous. Both conditions are, to a large extent, fulfilled by soft biological tissues specimens, such as those encountered in intraoperative imaging.

Tomographic reconstruction in cycloidal CT can be performed with standard methods, such as the filtered back projection (FBP) algorithm.

2.4 Samples

To explore the benefits of cycloidal CT for the intraoperative imaging of excised breast tissue, we scanned a human tumour-bearing breast tissue specimen obtained from the tissue bank at St. Bartholomew's Hospital (London, UK). The tissue was approximately 3 cm in width and depth and had been chemically fixed via immersion in paraformaldehyde for 24 h. It was wrapped in parafilm and placed in a cylindrical plastic container. For the exploration of oesophageal imaging, we scanned a tissue engineered oesophagus, generated through the *in vitro* maturation of a cell-seeded, pig-

derived, acellular scaffold[32,33]. The sample was approximately 4 mm in width and depth, and was contained in a plastic straw. This specific sample was used since it was the only oesophageal tissue available to us at the time (studied within our group in the context of a project on tissue engineering). While it cannot be considered representative of a human oesophagus (first and foremost due to substantial differences in size, but also, possibly, due to morphological differences which may pose additional challenges on the imaging process), we believe that the scan results can still inform on the utility of cycloidal CT for the imaging of biomedical samples more broadly.

2.5 Experimental setup and data acquisition

Scans were performed with an EI x-ray phase contrast imaging setup implemented on a breadboard in our UCL labs (see Fig. 3). The x-ray source is a Rigaku MicroMax 007 tube with a rotating molybdenum target, operated at 40 kVp and 20 mA, which presents a source focal spot size of approximately 70 µm (full-width half maximum) horizontally. The detector is a CMOS Hamamatsu C9732DK-11 flat panel, with 50 x 50 μm^2 pixels. The distance between the source and the detector is 85 cm, and the distance between the source and the sample is 70 cm, corresponding to a geometric magnification of about 1.21.

"Line skipping" masks were employed, which cover every other pixel column to effectively reduce crosstalk in the detector. The sample mask had a period of 79 µm and apertures of 12 µm, while the detector mask had apertures of 17 µm and a period of 98 µm. Both masks were manufactured by Creatv Microtec (USA) by electroplating gold onto a graphite substrate, resulting in a combination of absorbing and transmitting columns made of gold and graphite, respectively.

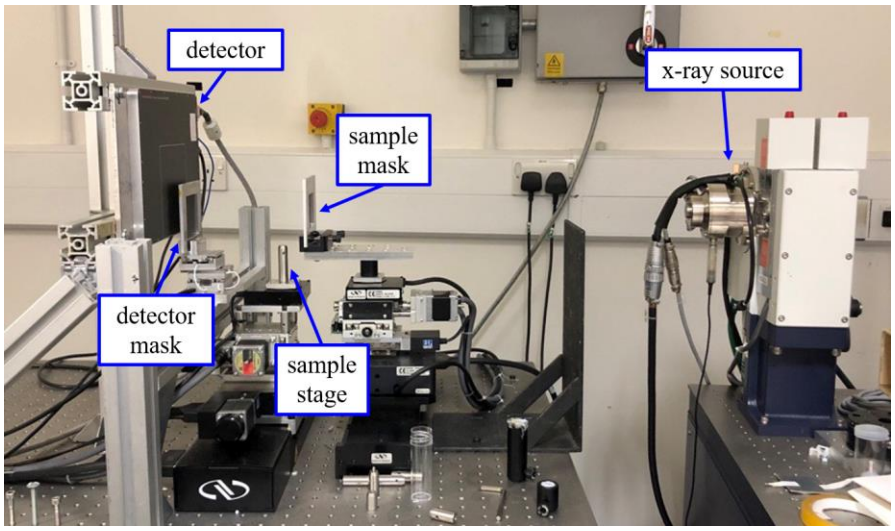

Figure 3. Photograph of the EI x-ray phase contrast imaging setup at UCL.

Fully sampled tomographic datasets were acquired through dithering; these were subsequently sub-sampled according to the grids shown in Figs. 2b and 2c to mimic rotation-only and cycloidal acquisitions. For the breast tissue specimen, 2500 projections were acquired as the sample was rotated over 360º, which corresponds to an angular sampling step of 0.144º. At each rotation angle, dithering was implemented by collecting 8 frames, each with the sample in a different subpixel position (at a different "dithering step"). A total of 2500 x 8 = 20000 frames were acquired, with an exposure time of 1.5 s each. For the oesophageal sample, 1000 projections were acquired over 360º, corresponding to an angular step of 0.36º. Again, dithering was applied involving 8 dithering steps. Hence, a total of 1000 x 8 = 8000 frames were acquired, with an exposure time of 1.2 s each.

The masks were positioned such that they had a lateral offset of 9 µm with respect to each other, which corresponds, approximately, to the steepest part of the illumination curve's left slope. Flat and dark fields images were also collected and used to perform gain and offset corrections on the raw projection data. The corrected projection data were assembled

into sinograms and bicubic splines interpolation was used to recover the missing entries in the sub-sampled datasets. Single-shot phase retrieval was employed to recover the phase function.

Tomographic slices were reconstructed using FBP after converting the sinograms from a fan-beam to a parallel-beam geometry using MATLAB's fan2para function. Since the setup has a cone beam geometry (rather than a fan-beam one), this approach is only valid for slices in the (vertical) centre of the cone.

3. RESULTS

The reconstructed images of the breast tissue specimen are shown in Figure 4. The individual panels show a fully sampled (i.e. dithered) image, an under-sampled image acquired with a rotation-only scheme, and an under-sampled image acquired with a cycloidal scheme, respectively. Unsurprisingly, the dithered image (panel a) exhibits the best quality in terms of spatial resolution and detail visibility, but it must be noted that this was reconstructed from eight times more data than the under-sampled images (panels b and c). While some degree of degradation in image quality can be observed in both under-sampled cases, the cycloidal image (panel c) appears to be sharper than the rotation-only image (panel b), although a distinct noise pattern obscures the visualization of small details. The structural similarity index measure (SSIM), calculated with the dithered image as a reference, is 0.37 for the rotation-only slice and 0.39 for the cycloidal slice.

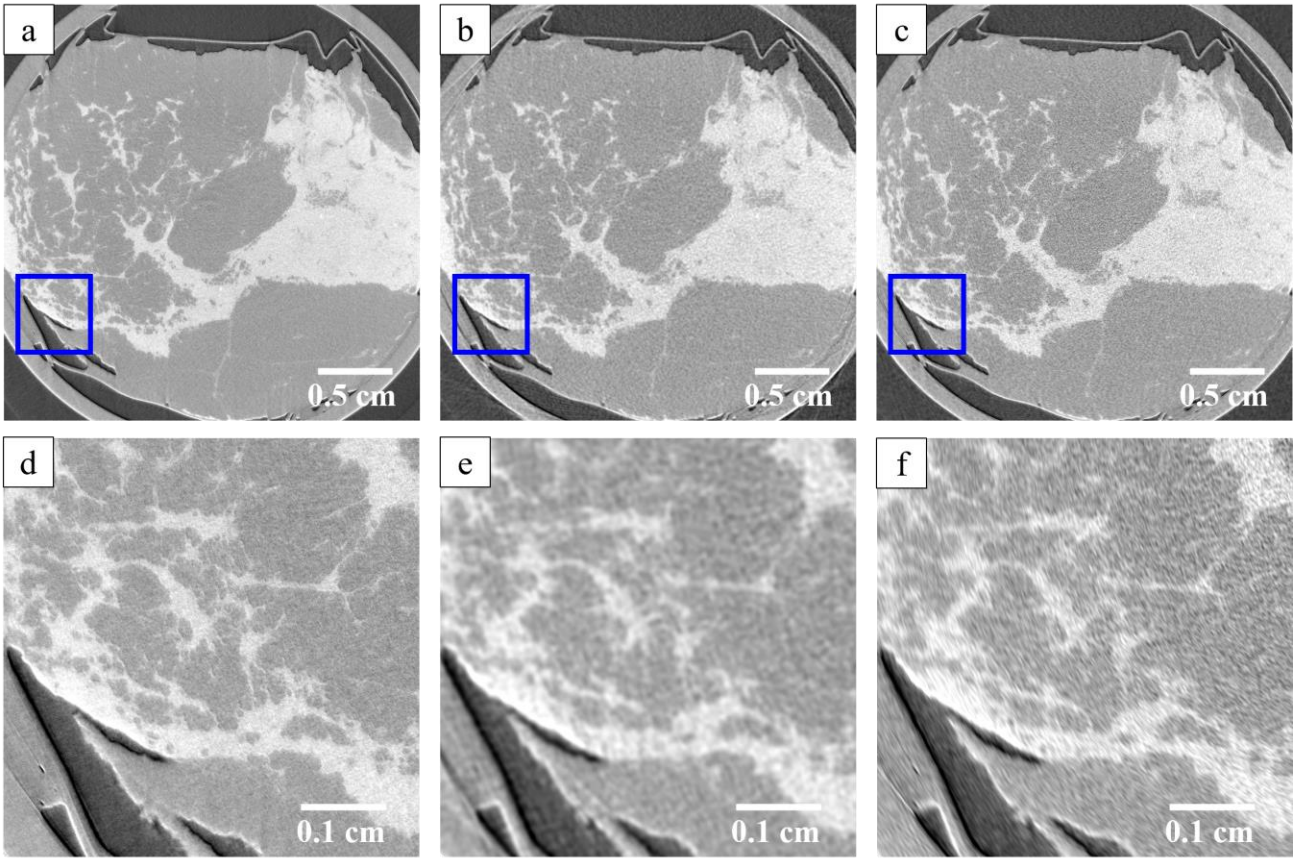

Figure 4. Reconstructed slices of a breast tissue specimen, and corresponding details of the tissue. Panels (a) and (d) show the fully dithered image, with 8 dithering steps. Panels (b) and (e) show the rotation-only image, which corresponds to having only 1 dithering step per projection, but without the lateral translation typical of cycloidal CT. Panels (c) and (f) show the cycloidal image.

The reconstructed tomographic images of the oesophagus are displayed in Figure 5. By and large, the same observations as for the breast tissue can be made. The dithered image exhibits the best image quality, with a spatial resolution of 18±3 µm, and again the cycloidal image in panel (c) shows a greatly improved resolution (24±5 µm) compared to the rotation-only case (70±10 µm). Resolution values were obtained by extracting edge spread functions across a number of marked areas (indicated in panel a but applied in the same manner in all images), fitting them with error functions, taking their derivative to arrive at line spread functions and extracting their full width half maxima. The resolution values extracted from each image were averaged, the stated error bars refer to the standard deviation. Visually, the different layers of tissue can be distinguished in the cycloidal image, which is hardly possible in the rotation-only image. At the same time, the cycloidal image reveals the same distinct noise texture that was observed above.

This has led us to investigate whether the integration of a CNN layer into the processing of the cycloidal images can improve their quality. For a detailed introduction to CNN-based image processing in cycloidal CT data we would like to refer to Ref. 28. In brief, a 100-layer mixed-scale dense (MS-D) CNN[34,35] was trained on 110 sinograms, with 18 sinograms as a validation set. The training was done by selecting a number (n=100) of fully sampled projections from the dithered sinograms, spaced in equal angular intervals of 3.6 degrees, which act as training target. The training input are the equivalent equally-spaced projections in the cycloidally sampled sinograms, with the missing data recovered via bicubic splines interpolation. The training data corresponds to 10% of the complete dataset. The CNN was trained for 96 h, and the training was restricted to the central region of the sinogram.

The cycloidal image processed with the additional CNN layer is shown in panel (d) of Fig. 5. Compared with panel (c), the noise texture appears to be smoother, while the spatial resolution remains comparable, at 24±4 µm. The interpolation approach has an SSIM of 0.66, compared to 0.73 with the MS-D CNN, which matches the visual improvements between panels (c) and (d). The rotation-only image, on the other hand, has a worse SSIM of 0.53 (all SSIM values are again based on the dithered image being the reference).

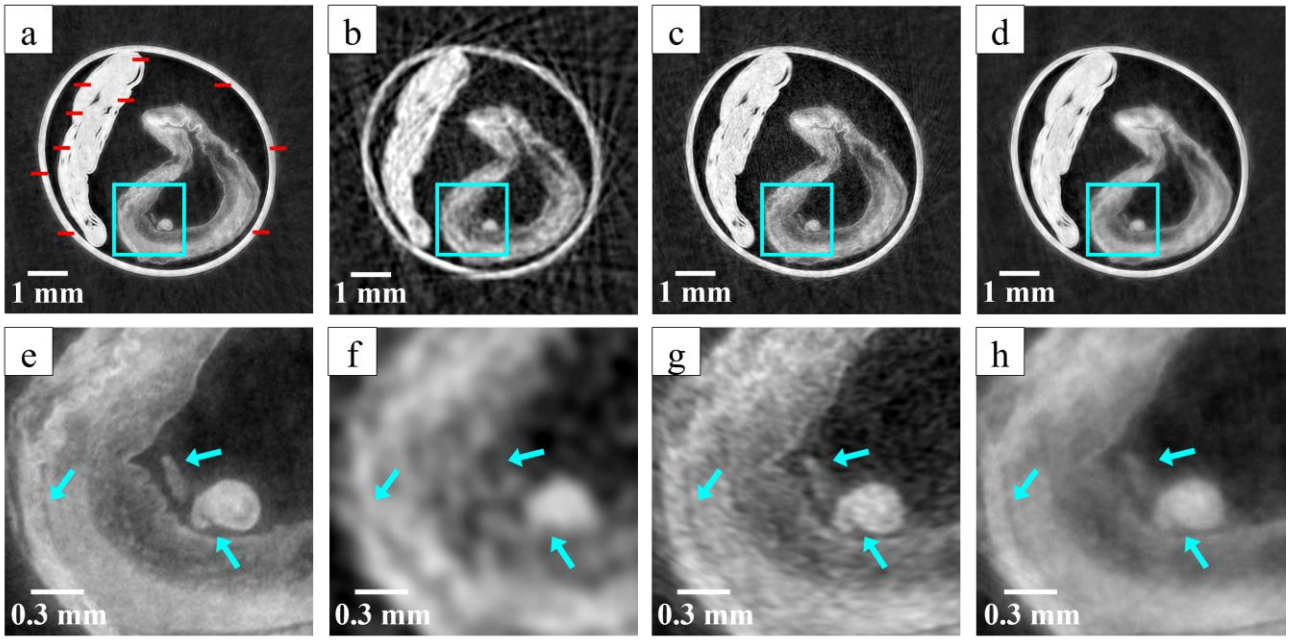

Figure 5. Reconstructed tomographic slices of a pig-derived tissue-engineered oesophagus, with zoomed-in details of the specimen. The bright elongated shape to the left of the oesophagus is parafilm. Panels (a) and (e) show the fully dithered image, with 8 dithering steps. Panel (a) also shows the areas where spatial resolution measurements were taken, in red. Panels (b) and (f) show the rotation-only image. Panels (c) and (g) show the cycloidal image, with the data recovery step done using bicubic splines interpolation. Additionally, panels (d) and (h) show a cycloidal image where data recovery is done in combination with an MS-D CNN. The light blue arrows on the bottom panels point at details that are lost in the rotation-only image but are visible in the cycloidal images.

4. DISCUSSION AND CONCLUSIONS

Cycloidal CT can provide high-resolution images within shorter scan times than dithering, or, vice versa, increase resolution over a rotation-only acquisition without the need for longer scans. It is a flexible approach that can be implemented in either attenuation or phase contrast configuration, which allows tailoring the contrast mode to the imaging needs of the sample being scanned. This is important in intraoperative specimen imaging, as surgically excised samples are often composed of soft tissue, which intrinsically exhibits weak x-ray attenuation and is therefore difficult to image with conventional x-ray techniques.

The results reported here indicate that cycloidal CT can be beneficial to intraoperative specimen imaging, especially when implemented in an EI x-ray phase contrast scanner. An increase in resolution was observed for both the breast tissue sample and the oesophagus when cycloidal sampling was applied rather than a rotation-only scheme. Image quality in the dithered images, which can be considered a gold-standard reference, is, unsurprisingly, better. But the difference must be weighed up against the fact that a much larger amount of data are acquired with dithering (e.g., eight times more in the examples shown here). Not only does this lengthen scan time per se (unless the exposure time per frame is reduced), but dithered scans are also bound to be step-and-shoot scans, as the sample must remain in a fixed angular position while the lateral subpixel steps are acquired. In step-and-shoot scans, the repeated stop-starting of the rotation and translation motors can lead to significant overheads. On the contrary, cycloidal acquisitions can be realized as flyscans[27], where the sample is simultaneously rotated and translated without interruption. Provided that the detector integration time is negligible, overheads are removed and scan time is equal to exposure time.

In conclusion, our preliminary results are promising but further research is needed to fully establish the potential of cycloidal CT for intraoperative specimen imaging. Our next steps will include scanning further samples and comparing the results against histological slices. We will then work towards implementing cycloidal CT with the dedicated scanners that were developed by our group for the intraoperative margin assessment of resected tumours. We believe that the application of cycloidal sampling will relax the relationship between resolution and scan time, which is currently a limiting factor. Some scanner adaptations may be necessary; specifically, the cycloidal method requires that the beamlets are sufficiently separated as otherwise they would “blur” and high-resolution information be lost. Considering the intraoperative scanner reported in Ref. 5 as an example, this uses a “non-line skipping” sample mask, which means that every column of the detector is illuminated by a beamlet. However, crosstalk in the detector means that signals are spread across neighbouring pixels, which has a similarly detrimental effect as insufficiently separated beamlets. To reduce the crosstalk, that scanner may need to be fitted with a “line skipping” sample mask.

In terms of data processing, the application of a CNN layer to restore under-sampled cycloidal sinograms shows promise but needs further investigation before being suitable to in-theatre use. The main limitation currently is that the time it takes to train the network far exceeds the time constraints of intraoperative imaging (in our specific example, the network was trained for 96 h). However, until now, we have trained a unique CNN for each sample specifically, based on training projections which were interleaved within the cycloidal sampling scheme. A more suitable alternative may be to train a CNN “offline” based on images of samples that were scanned previously, and then apply the trained network to any subsequent samples that are scanned intraoperatively.

REFERENCES

[1] Cabioglu, N., Hunt, K. K., Sahin, A. A., Kuerer, H. M., Babiera, G. V., Singletary, S. E., Whitman, G. J., Ross, M. I., Ames, F. C., Feig, B. W., et al., “Role for intraoperative margin assessment in patients undergoing breast-conserving surgery," Annals of Surgical Oncology 14(4), 1458-1471 (2007).

[2] John, E.S., Al-Khudairi, R., Ashrafian, H., Athanasiou, T., Takats, Z., Hadjiminas, D., Darzi, A., Leff, D., “Diagnostic accuracy of intraoperative techniques for margin assessment in breast cancer surgery”, Annals of Surgery 265, 300–10 (2017).

[3] Massimi, L., Hagen, C. K., Endrizzi, M., Munro, P. R. T., Havariyoun, G., Hawker, P. M. S., Smit, B., Astolfo, A., Larkin, O. J., Waltham, R. M. et al., “Laboratory-based x-ray phase contrast CT technology for clinical intra-operative specimen imaging”, Proc. SPIE 10948, Medical Imaging 2010: Physics of Medical Imaging, 109481R (2019).

[4] Havariyoun, G., Vittoria, F. A., Hagen, C. K., Basta, D., Kallon, G., Endrizzi, M., Massimi, L., Munro, P. R. T., Hawker, P. M. S., Smit, B. et al., "A compact system for intraoperative specimen imaging based on edge illumination x-ray phase contrast," Physics in Medicine and Biology 64, 235005 (2019).
[5] Massimi, L., Suaris, T., Hagen, C. K., Endrizzi, M., Munro, P. R. T., Havariyoung, G., Hawker, P. M. S., Smit, B. et al, "Detection of involved margins in breast specimens with x-ray phase-contrast computed tomography," Sci. Rep. 11(1), 3663 (2021).
[6] Hagen, C. K., Vittoria, F. A., Roche i Morgo, O., Endrizzi, M., Olivo, A., "Cycloidal computed tomography", Physical Review Applied 14, 014069 (2020).
[7] Van Dongen, J. A., Voogd, A. C., Fentiman, I. S., et al. "Long-term results of a randomized trial comparing breast-conserving therapy with mastectomy: European Organization for Research and Treatment of Cancer 10801 trial," J Natl Cancer Inst, 92(14), 1143–50 (2000).
[8] Arriagada, R., Le, M. G., Rochard, F., Contesso, G. "Conservative treatment versus mastectomy in early breast cancer: patterns of failure with 15 years of follow-up data," Institut Gustave-Roussy Breast Cancer Group, J Clin Oncol, 14(5), 1558–64 (1996).
[9] Safranek, P. M., Cubitt, J., Booth, M. I., Dehn, T. C., "Review of open and minimal access approaches to oesophagectomy for cancer," British Journal of Surgery, 97(12), 1845–5 (2010).
[10] Luketich, J. D., Pennathur, A., Awais, O., et al. "Outcomes after minimally invasive esophagectomy: review of over 1000 patients," Ann Surg 256(1), 95-103 (2012).
[11] Endrizzi. M, "X-ray phase contrast imaging", Nuclear Instruments and Methods in Physics Research Section A: Accelerators, Spectrometers, Detectors and Associated Equipment, 878, 88-98 (2018).
[12] Wilkins S., Nesterets Y. I., Gureyev T., Mayo S., Pogany A., Stevenson A., "On the evolution and relative merits of hard x-ray phase-contrast imaging methods," Philosophical Transactions of the Royal Society of London A: Mathematical, Physical and Engineering Sciences, 372, 20130021, (2010) (2014).
[13] Momose A., Takeda T., Itai Y., and Hirano K., "Phase-contrast X-ray computed tomography for observing biological soft tissues," Nat. Med. 2(4), 473–475 (1996).
[14] Momose A., Takeda T., Itai Y., "Phase-contrast x-ray computed tomography for observing biological specimens and organic materials," Review of scientific instruments 66(2), 1434–1436, (1995).
[15] Massimi, L., Bukreeva, I., Santamaria, G., Fratini, M., Corbelli, A., Brun, F., Fumagalli, S., Maugeri, L., Pacureanu, A., Cloetens, P., et al., "Exploring Alzheimer's disease mouse brain through x-ray phase contrast tomography: From the cell to the organ," NeuroImage 184, 490-495 (2019).
[16] Mittone, A., Ivanishko, Y., Kovalev, S., Lisutina, P., Lotoshnikov, M., Tkachev, S., Tkacheva, M., Crippa, L., Dmitriev, V., and Bravin, A., "High resolution hard x-ray 3d mapping of a macaca fascicularis eye: A feasibility study without contrast agents," Physica Medica 51, 7-12 (2018).
[17] Massimi, L., Meganck, J. A., Towns, R., Olivo, A. and Endrizzi, M., "Evaluation of a compact multicontrast and multiresolution x-ray phase contrast edge illumination system for small animal imaging", Med. Phys. 48(1), 376-386 (2021).
[18] Olivo, A. and Speller, R. "A coded-aperture technique allowing x-ray phase contrast imaging with laboratory sources" Appl. Phys. Lett. 91(7), 074106 (2007).
[19] Olivo, A., Arvanitis, C., Bohndiek, S., Clark, A., Prydderch, M., Turchetta, R. and Speller, R. "First evidence of phase contrast imaging with laboratory sources and active pixel sensors," Nucl. Instrum. Meth. A 581(3), 776-82 (2007).
[20] Ignatyev, K., Munro, P. R. T., Chana, D., Speller, R. D. and Olivo, A. "Coded apertures allow high-energy x-ray phase contrast imaging with laboratory sources," J. Appl. Phys. 110(1), 014906 (2011).
[21] Diemoz, P. C., Hagen, C. K., Endrizzi, M. and Olivo, A., "Sensitivity of laboratory based implementations of edge illumination x-ray phase-contrast imaging," Appl. Phys. Lett. 103(24) 244104 (2013).
[22] Olivo, A. and Speller, R., "Modelling of a novel x-ray phase contrast imaging technique based on coded apertures," Phys Med Biol, 52(22), 6555-6573 (2007).
[23] Diemoz, P. C. and Olivo, A., "On the origin of contrast in edge illumination X-ray phase-contrast imaging," Opt Express, 22(23), 28199-28214 (2014).
[24] Diemoz, P. C., Endrizzi, M., Bravin, A., Robinson I. K., and Olivo, A., "Sensitivity of edge-illumination x-ray phase contrast imaging," Phil. Trans. R. Soc. A., 372 (2014).
[25] Hagen, C. K., Vittoria, F. A., Endrizzi, M. and Olivo, A., "Theoretical framework for spatial resolution in edge-illumination x-ray tomography," Phys. Rev. Appl. 10, 054050 (2018).

[26] Diemoz, P. C., Vittoria, F. A. and Olivo, A., "Spatial resolution of edge illumination X-ray phase-contrast imaging," Opt. Exp., 22, 15514-29 (2014).
[27] Roche i Morgo, O., Vittoria, F., Endrizzi, M., Olivo, A. and Hagen, C. K., "Technical Note: Practical implementation strategies of cycloidal computed tomography," Med. Phys. Special Issue Paper, https://doi-org.libproxy.ucl.ac.uk/10.1002/mp.14821, (2021).
[28] Pelt, D. M, Maughan-Jones, C., Roche i Morgo, O., Olivo, A. and Hagen, C. K., "Rapid and flexible high-resolution scanning enabled by cycloidal computed tomography and convolutional neural network (CNN) based data recovery," Proc. 6th International Conference on Image Formation in X-Ray Computed Tomography, Regensburg, Germany (virtual), 3-7 Aug 2020, pp. 86-89.
[29] Zamir, A., Endrizzi, M., Hagen, C. K., et al., "Robust phase retrieval for high resolution edge illumination x-ray phase-contrast computed tomography in non-ideal environments," Sci Rep. 6, 31197 (2016).
[30] Diemoz, P. C., Hagen, C. K., Endrizzi, M., et al. "Single-shot x-ray phase-contrast computed tomography with non-microfocal laboratory sources," Phys Rev Appl. 7(4), 044029 (2017).
[31] Diemoz, P. C., Vittoria, F. A., Hagen, C. K., et al. "A single-image retrieval method for Edge illumination x-ray phase-contrast imaging: application and noise analysis," Phys Med., 32(12), 17598-1764 (2016).
[32] Totonelli, G. et al. "Detergent enzymatic treatment for the development of a natural acellular matrix for oesophageal regeneration," Pediatr. Surg. Int. 29(1), 87–95 (2013).
[33] Urbani, L. Camilli, C., Phylactopoulos, D. E., Crowley, C., Natarajan, D., Scottoni, F., et al. "Multi-stage bioengineering of a layered oesophagus with in vitro expanded muscle and epithelial adult progenitors," Nat. Commun. 9, 4286 (2018).
[34] Pelt, D. M. and Sethian, J. A., "A mixed-scale dense convolutional neural network for image analysis," Proc. Natl. Acad. Sci., U.S.A., 115, 254-259 (2018).
[35] Pelt, D. M., Batenburg, K. J., and Sethian, J. A., "Improving tomographic reconstruction from limited data using mixed-scale dense convolutional neural networks", J. Imaging, 4(11), 128 (2018).

ACKNOWLEDGMENTS

This work is supported by the Wellcome/EPSRC Centre for Interventional and Surgical Sciences (WEISS) (203145/Z/16/Z). Additional funding by the Wellcome Trust [200137/Z/15/Z] and by EPSRC [EP/T005408/1] is acknowledged. C. K. Hagen is supported by the Royal Academy of Engineering, under the Research Fellowship scheme. A. Olivo is supported by the Royal Academy of Engineering, under the Chair in Emerging Technologies scheme. P. R. T. Munro is funded by the Royal Society under the University Research Fellowships scheme. S. Savvidis was supported by the EPSRC-funded UCL Centre for Doctoral Training in Medical Imaging (EP/L016478/1). D. M. Pelt is supported by The Netherlands Organisation for Scientific Research (NWO), project number 016.Veni.192.235. The authors wish to acknowledge the roles of the Breast Cancer Now Tissue Bank in collecting and making available the samples, and the patients who have generously donated the tissues which have been utilised in the generation of this publication.